PRINCIPLES OF INORGANIC MATERIALS DESIGN

John. N. Lalena
Consultant
Formerly Senior Research Scientist
Honeywell Electronic Materials

David. A. Cleary
Chairman, Department of Chemistry
Gonzaga University

WILEY-INTERSCIENCE
A JOHN WILEY & SONS, INC., PUBLICATION

PRINCIPLES OF INORGANIC MATERIALS DESIGN

PRINCIPLES OF INORGANIC MATERIALS DESIGN

John. N. Lalena
Consultant
Formerly Senior Research Scientist
Honeywell Electronic Materials

David. A. Cleary
Chairman, Department of Chemistry
Gonzaga University

WILEY-INTERSCIENCE
A JOHN WILEY & SONS, INC., PUBLICATION

Published by John Wiley & Sons, Inc., Hoboken, New Jersey.
Published simultaneously in Canada.

Library of Congress Cataloging-in-Publication Data is Available

0-471-43418-3

Printed in the United States of America

10 9 8 7 6 5 4 3 2 1

To our families

CONTENTS

FOREWORD

Whereas solid-state physics is concerned with the mathematical description of the varied physical phenomena that solids exhibit and the solid-state chemist is interested in probing the relationships between structural chemistry and physical phenomena, the materials scientist has the task of using these descriptions and relationships to design materials that will perform specified engineering functions. However, the physicist and the chemist are often called on to act as material designers, and the practice of materials design commonly requires the exploration of novel chemistry that may lead to the discovery of physical phenomena of fundamental importance for the body of solid-state physics. I cite three illustrations where an engineering need has led to new physics and chemistry in the course of materials design.

In 1952, I joined a group at the M.I.T. Lincoln Laboratory that had been charged with the task of developing a square *B–H* hysteresis loop in a ceramic ferrospinel that could have its magnetization reversed in less than 1 μs by an applied magnetic-field strength less than twice the coercive field strength. At that time, the phenomenon of a square *B–H* loop had been obtained in a few iron alloys by rolling them into tapes so as to align the grains, and hence the easy magnetization directions, along the axis of the tape. The observation of a square *B–H* loop led Jay Forrester, an electrical engineer, to invent the coincident-current, random-access magnetic memory for the digital computer since, at that time, the only memory available was a 16×16 byte electrostatic storage tube. Unfortunately, the alloy tapes gave too slow a switching speed. As an electrical engineer, Jay Forrester assumed the problem was eddy-current losses in the tapes, so he had turned to the ferrimagnetic ferrospinels that were known to be magnetic insulators. However, the polycrystalline ferrospinels are ceramics that cannot be rolled! Nevertheless, the U.S. Air Force had financed the M.I.T. Lincoln Laboratory to develop an Air Defense System, of which the digital computer was to be a key component. Therefore, Jay Forrester was able to put together an interdisciplinary team of electrical engineers, ceramists, and physicists to realize his random-access magnetic memory with ceramic ferrospinels.

The magnetic memory was achieved by a combination of systematic empiricism, careful materials characterization, theoretical analysis, and the emergence of an unanticipated phenomenon that proved to be a stroke of good fortune. A systematic mapping of the structural, magnetic, and switching properties of the Mg–Mn–Fe

ferrospinels as a function of their heat treatments revealed that the spinels in one part of the phase diagram were tetragonal rather than cubic and that compositions just on the cubic side of the cubic-tetragonal phase boundary yield sufficiently square *B–H* loops if given a carefully controlled heat treatment. This observation led me to propose that the tetragonal distortion was due to a cooperative orbital ordering on the Mn^{3+} ions that would lift the cubic-field orbital degeneracy; cooperativity of the site distortions minimizes the cost in elastic energy and leads to a distortion of the entire structure. This phenomenon is now known as a cooperative Jahn–Teller distortion since Jahn and Teller had earlier pointed out that a molecule or molecular complex having an orbital degeneracy would lower its energy by deforming its configuration to a lower symmetry that removed the degeneracy. Armed with this concept, I was able almost immediately to apply it to interpret the structure and the anisotropic magnetic interactions that had been found in the manganese-oxide perovskites, since the orbital order revealed the basis for specifying the rules for the sign of a magnetic interaction in terms of the occupancies of the overlapping orbitals responsible for the interatomic interactions. These rules are now known as the Goodenough–Kanamori rules for the sign of a superexchange interaction. Thus an engineering problem prompted the discovery and description of two fundamental phenomena in solids that have ever since been used by chemists and physicists to interpret structural and magnetic phenomena in transition-metal compounds and to design new magnetic materials. Moreover, the discovery of cooperative orbital ordering fed back to an understanding of our empirical solution to the engineering problem. By annealing at the optimum temperature for a specified time, the Mn^{3+} ions of a cubic spinel would migrate to form Mn-rich regions where their energy is lowered through cooperative, dynamic orbital ordering. The resulting chemical inhomogeneities acted as nucleating centers for domains of reverse magnetization that, once nucleated, grew away from the nucleating center. We also showed that eddy currents were not responsible for the slow switching of the tapes, but a small coercive field strength and an intrinsic damping factor for spin rotation.

In the early 1970s, an oil shortage focused worldwide attention on the need to develop alternative energy sources, and it soon became apparent that these sources would benefit from energy storage. Moreover, replacing the internal combustion engine with electric-powered vehicles, or at least the introduction of hybrid vehicles, would improve the air quality, particularly in big cities. Therefore, a proposal by the Ford Motor Company to develop a sodium–sulfur battery operating at 300°C with molten electrodes and a ceramic Na^+-ion electrolyte stimulated interest in the design of fast alkali-ion conductors. More significant was interest in a battery in which Li^+ rather than H^+ is the working ion, since the energy density that can be achieved with an aqueous electrolyte is lower than what, in principle, can be obtained with a nonaqueous Li^+-ion electrolyte. However, realization of a Li^+-ion rechargeable battery would require identification of a cathode material into/from which Li^+ ions can be inserted/extracted reversibly. Brian Steele of Imperial College, London, first suggested use of TiS_2, which contains TiS_2 layers held together only by Vander Waals S^{2-}—S^{2-} bonding; lithium can be inserted

reversibly between the TiS_2 layers. M. Stanley Whittingham's demonstration was the first to reduce this suggestion to practice while he was at the Exxon Corporation. Whittingham's demonstration of a rechargeable Li–TiS_2 battery was commercially nonviable because the lithium anode proved unsafe. Nevertheless, his demonstration focused attention on the work of the chemists Jean Rouxel of Nantes, France, and R. Schöllhorn of Berlin on insertion compounds that provide a convenient means of changing continuously the mixed valency of a fixed transition-metal array across a redox couple. Although work at Exxon was halted, their demonstration had shown that if an insertion compound such as graphite were used as the anode, a viable lithium battery could be achieved, but use of a less electropositive anode would require an alternative insertion-compound cathode material that provided a higher voltage vs. a lithium anode than TiS_2. I was able to deduce that no sulfide would give a significantly higher voltage than that obtained with TiS_2 and therefore that it would be necessary to go to a transition-metal oxide. Although oxides other than V_2O_5 and MoO_3, which contain vandyl or molybdyl ions, do not form layered structures analogous to TiS_2, I knew that $LiMO_2$ compounds exist that have a layered structure similar to that of $LiTiS_2$. It was only necessary to choose the correct M^{3+} cation and to determine how much Li could be extracted before the structure collapsed. That was how the $Li_{1-x}CoO_2$ cathode material was developed that now powers the cell telephones and laptop computers. The choice of M = Co, Ni, or $Ni_{0.5+\delta}Mn_{0.5-\delta}$ was dictated by the position of the redox energies and an octahedral site-preference energy strong enough to inhibit migration of the M atom to the Li layers on removal of Li. Electrochemical studies of these cathode materials, and particularly of $Li_{1-x}Ni_{0.5+\delta}Mn_{0.5-\delta}O_2$, have provided a demonstration of the pinning of a redox couple at the top of the valence band, a concept of singular importance for interpretation of metallic oxides having only M–O–M interactions, of the reason for oxygen evolution at critical Co(IV)/Co(III) or Ni(IV)/Ni(III) ratios in $Li_{1-x}MO_2$ studies, and of why Cu(III) in an oxide has a low-spin configuration. Moreover, exploration of other oxide structures that can act as hosts for insertion of Li as a guest species have provided a means of quantitatively determining the influence of a countercation on the energy of a transition-metal redox couple. This determination allows tuning of the energy of a redox couple, which may prove important for the design of heterogenous catalysts.

As a third example, I turn to the discovery of high-temperature superconductivity in the copper oxides first announced by Bednorz and Müller of IBM Zürich in the summer of 1986. Karl A. Müller, the physicist of the pair, had been thinking that a dynamic Jahn–Teller ordering might provide an enhanced electron–phonon coupling that would raise the superconductive critical temperature T_C. He turned to his chemist colleague Bednorz to make a mixed-valent Cu^{3+}/Cu^{2+} compound, since Cu^{2+} has an orbital degeneracy in an octahedral site. This speculation led to the discovery of the family of high-T_C copper oxides; however, the enhanced electron–phonon coupling is not due to a conventional dynamic Jahn–Teller orbital ordering, but rather to the first-order character of the transition from localized to itinerant electronic behavior of σ-bonding Cu:3d electrons of $(x^2 - y^2)$ symmetry in CuO_2 planes. In this case, the search for an improved engineering material has led

to a demonstration that the celebrated Mott–Hubbard transition is generally not smooth as originally assumed, and it has introduced an unanticipated new physics associated with bond-length fluctuations and vibronic electronic properties. It has challenged the theorist to develop new theories of the crossover regime that can describe the mechanism of superconductive pair formation in the copper oxides, quantum critical-point behavior at low temperatures, and an anomalous temperature dependence of the resistivity at higher temperatures as a result of strong electron–phonon interactions.

These examples show how the challenge of materials design from the engineer may lead to new physics as well as to new chemistry. Sorting out the physical and chemical origins of the new phenomena feed back to the range of concepts available to the designer of new engineering materials. In recognition of the critical role in materials design of interdisciplinary cooperation between physicists, chemists, ceramists, metallergists, and engineers that is practiced in industry and government research laboratories, John N. Lalena and David A. Cleary have initiated with their book what should prove to be a growing trend toward greater interdisciplinarity in the education of those who will be engaged in the design and characterization of tomorrow's engineering materials.

JOHN B. GOODENOUGH

Virginia H. Cockrell Centennial Chair in Engineering
The University of Texas at Austin

PREFACE

Inorganic solid-state chemistry has matured into its own distinct subdiscipline. The reader may wonder why we have decided to add another textbook to the plethora of books already published. Our response is that we see a need for a single-source presentation that recognizes the interdisciplinary nature of the field. Solid-state chemists typically receive a small amount of training in condensed-matter physics, but none in materials science or engineering, and yet all of these traditional fields are inextricable components of inorganic solid-state chemistry.

Materials scientists and engineers have traditionally been primarily concerned with the fabrication and utilization of materials already synthesized by the chemist and identified by the physicist as having the appropriate intrinsic properties for a particular engineering function. Although the demarcation between the three disciplines remains in an academic sense, the separate job distinctions for those working in the field are fading. This is especially obvious in the private sector, where one must ensure that materials used in real commercial devices not only perform their primary function, but also meet a variety of secondary requirements.

Individuals involved with such multidisciplinary projects must be prepared to work independently or to collaborate with other specialists in facing design challenges. In the latter case, communication is enhanced, if each individual is able to speak the ''language'' of the other. Therefore, in this book we introduce a number of concepts that are not usually covered in standard solid-state chemistry textbooks. When this occurs, we try to follow the introduction of the concept with an appropriate worked example to demonstrate its use. Two areas that have lacked thorough coverage in most solid-state chemistry texts in the past, namely, microstructure and mechanical properties, are treated extensively in this book.

We have kept the mathematics to a minimum—but adequate—level, suitable for a descriptive treatment. Appropriate citations are included for those needing the quantitative details. It is assumed that the reader has sufficient knowledge of calculus and elementary linear algebra, particularly matrix manipulations, and some prior exposure to thermodynamics, quantum theory, and group theory. The book should be satisfactory for senior-level undergraduate or beginning graduate students in chemistry. One will recognize from the Table of Contents that entire textbooks have been devoted to each of the chapters in this book, which indicates the necessary limits on the depth of coverage. Along with their chemistry colleagues,

physics and engineering students should also find the book to be informative and useful.

Every attempt has been made to extensively cite all the original and pertinent research in a fashion similar to that found in a review article. Students are encouraged to seek out this work. We have also included biographies of several individuals who have made significant *fundamental* contributions to inorganic materials science in the twentieth century. Limiting these to the small number we have room for was, of course, difficult. The reader should be warned that some topics have been left out. In this book, we only cover nonmolecular inorganic materials. Polymers and other molecular substances are not discussed. Also omitted are coverages of surface science, self-assembly, and composite materials.

We are grateful to Prof. John B. Wiley, Dr. Nancy F. Dean, Dr. Martin W. Weiser, Dr. Everett E. Carpenter, and Dr. Thomas K. Kodenkandath for reviewing various chapters in this book. We are grateful to Prof. John F. Nye, Prof. John B. Goodenough, Dr. Frans Spaepen, Dr. Larry Kaufman, and Dr. Bert Chamberland for providing biographical information. We also thank Prof. Philip Andersn, Prof. Mats H. Hillert, Prof. Nye, Dr. Kaufman, Dr. Terrell Vanderah, Dr. Barbara Sewall, and Mrs. Jennifer Moss for allowing us to use photographs from their personal collections. Finally, we acknowledge the inevitable neglect our families must have felt during the period taken to write this book. We are grateful for their understanding and tolerance.

CHAPTER 1

The Mesoscale

The prefix *meso-* comes from the Greek *mesos*, meaning ''intermediate'' or ''in the middle.'' Materials scientists and engineers describe the structure of a substance at four different length scales: macroscopic > mesocopic > microscopic > molecular/nano level. Sometimes the labels for the two intermediate levels are interchanged. To avoid confusion in this textbook, we group these two levels into one ''meso'' length scale between the nano- and macroscopic levels.

Before the advent of X-ray diffractometry, mineralogists could only visually examine crystals. An entire classification scheme was developed and still in use today for describing a single crystal's external morphology, or macroscopic appearance. One or more of 47 possible *forms* are usually apparent in the morphology. A form is a collection of symmetry-equivalent faces. The crystal *habit*, which depends on the relative sizes of the faces of the various forms present, may be described as cubic, octahedral, fibrous, acicular, prismatic, dendritic (tree-like), platy, or blade-like, among others. If a crystal is grown in a symmetrical environment, for example, freely suspended in a liquid, its morphological symmetry is exactly that of the point group *isogonal* (same angular relation) with its space group. It will depart from true point group symmetry under nonsymmetrical growth conditions.

With conventionally processed polycrystals, the smallest particles that are discernible with a high-quality optical microscope are the individual crystallites, or grains, that make up the sample. The term *microstructure* refers to the grain morphology, or grain size, shape, and orientation. Different techniques may be used to examine specific structural features. For example, high-resolution imaging with a scanning electron microscope (SEM) enables observation of dislocations. Information about preferred orientation can be obtained with an X-ray diffractometer equipped with a texture goniometer or by electron backscattered diffraction (EBSD).

Given the penetration depths in Table 1.1, it is obvious that electron diffraction and microscopy only probe the surfaces of solids (the topmost atomic layers), whereas neutron and X-ray diffraction provide information about the bulk. It is well known that the surface crystalline structure of a solid may differ from that of the bulk. The surfaces of most samples, however, are usually subjected to some sort of

Principles of Inorganic Materials Design By John N. Lalena and David A. Cleary
ISBN 0-471-43418-3

TABLE 1.1 Some Probes Used in Materials Characterization

Source	Wavelength[a] (Å)	Penetration Depth
Light	4×10^3–7×10^3	0
Neutrons	1–2.5	cm–dm
X-rays	0.1–10	μm–mm
Electrons	0.04	nm

[a] For elementary particles, $\lambda = hc/\sqrt{(2mc^2E)}$; for light and X-rays, $\lambda = hc/E$.

chemical–mechanical polishing prior to microstructural analysis to ensure that bulk grain morphology is apparent.

Inorganic materials are commonly grouped into one of two structure categories: crystalline or amorphous (glassy). Amorphous materials possess no long-range structural order, or periodicity. By contrast, crystalline solids are composed of arrays of atoms or molecules, whose positions may be referenced to a translationally invariant lattice. All crystals possess one or more of the basic symmetry elements. Some authors also classify fractals as a distinct structural class. In this case, the structure is self-similar, or scale-invariant, looking identical at all length scales (e.g., cauliflowers and silica aerogels). Crystal structure, however, is the topic of the next chapter. In this chapter, we focus on the microstructures of polycrystalline solids. The majority of solid materials of technological interest are used in polycrystalline form.

Microstructure is determined by the conditions used during the material processing. Hence, our objective is to clarify that a major goal of inorganic materials engineering is the systematic generation of specific grain morphologies in order to vary and adapt the properties of polycrystalline materials to given applications. We focus on describing the microstructures of solidification products (metals), formed powder aggregates (ceramics), and thin films. Microstructure/property correlation is also discussed. Mechanical, chemical, and transport properties are markedly influenced by microstructure.

1.1 INTERFACES IN POLYCRYSTALS

The regions separating different grains, or crystallites, within a polycrystalline solid are called *grain boundaries*. Although grain boundaries are often regarded as regions of structural disorder, it is now well established that many have a periodic structure. True incoherency, in which there is little correlation between atomic positions across the boundary, only sets in when the mismatch between adjacent crystals is very high (Bhadeshia, 1987). This is primarily determined by the relative orientations of the adjoining grains. In a polycrystalline sample, both the grain orientation distribution, or *texture*, and the structure of the grain boundary itself can be crucial to the bulk materials properties. Therefore, it is appropriate to begin with orientation relationships.

1.1.1 Orientation Relationships in Bicrystals

The orientation relationship between a pair of grains of the same substance (the only kind we will consider here), a *bicrystal*, is often expressed by an axis-angle description, since one crystal always can be generated from the other by a rigid-body rotation about a suitable axis. More precisely, the lattices can be made to coincide by turning one of the crystals about a suitable rotation axis. Rotation axes are commonly denoted as unit vectors, in terms of three indices of direction written in square brackets, [*uvw*], while the misorientation angle is expressed in degrees about this axis. The [*uvw*] indices are obtained by taking the projections of the vector on the *x*, *y*, and *z*-axes, respectively, of a Cartesian coordinate system and dividing these three numbers by their highest common denominator.

It is always possible to describe the orientation relationship between a pair of grains in terms of more than one axis-angle pair. Consider a pair of adjacent identical cubic crystals of different orientation, *A* and *B*. Suppose further that *B* can be generated from *A* by a right-hand rotation of 60° counterclockwise about the *A* crystal's body-diagonal axis, or the $[111]_A$ direction. This particular orientation relationship is called a *twin*, since the two domains are related by a symmetry element (a twin operation) that is not part of the space group symmetry of a single crystal of the material. The extra symmetry element may be a reflection plane (twin plane) or a rotation axis (twin axis). The high symmetry of the cubic lattice allows us to find numerous equivalent axis-angle pairs for any orientation relationship. Using this twin boundary as an example, we now show how other axis-angle pairs, which are equivalent to a 60° right-hand rotation about the $[111]_A$ axis, can be obtained.

Indices are convenient for describing directions (vectors or axes) in crystals. However, direction cosines are much more useful for calculations. Therefore, one must first convert the direction indices, [*uvw*], designating the rotation axis into direction cosines. In our present example, the body diagonal of a cube of unit length has direction indices [111]. This is seen by using a Cartesian coordinate system, where the origin of the cube is taken to be one of its corners and which is designated as $(x_1, y_1, z_1) = (0, 0, 0)$. The body diagonal is obtained by drawing a line segment of length $|\boldsymbol{r}|$ from the origin and terminating at the coordinates $(x_2, y_2, z_2) = (1, 1, 1)$. The direction cosines are given by the equations:

$$\begin{aligned} \cos\alpha &= r_1 = (x_2 - x_1)/|\,\boldsymbol{r}\,| \\ \cos\beta &= r_2 = (y_2 - y_1)/|\,\boldsymbol{r}\,| \\ \cos\gamma &= r_3 = (z_2 - z_1)/|\,\boldsymbol{r}\,| \end{aligned} \tag{1.1}$$

where $|\boldsymbol{r}|$ is given by $[r_1^2 + r_2^2 + r_3^2]^{1/2} = [(x_2 - x_1)^2 + (y_2 - y_1)^2 + (z_2 - z_1)^2]^{1/2}$. Hence, in the cubic crystal, we get $\cos\alpha = \cos\beta = \cos\gamma = 0.5773$, satisfying the requirement that $\cos^2\alpha + \cos^2\beta + \cos^2\gamma = 1$.

A (3×3) square rotation matrix, $\mathbf{R}$, may now be obtained, which has the following elements:

$$\begin{pmatrix} r_1r_1(1-\cos\theta)+\cos\theta & r_1r_2(1-\cos\theta)+r_3\sin\theta & r_1r_3(1-\cos\theta)-r_2\sin\theta \\ r_1r_2(1-\cos\theta)-r_3\sin\theta & r_2r_2(1-\cos\theta)+\cos\theta & r_2r_3(1-\cos\theta)+r_1\sin\theta \\ r_1r_3(1-\cos\theta)+r_2\sin\theta & r_2r_3(1-\cos\theta)-r_1\sin\theta & r_3r_3(1-\cos\theta)+\cos\theta \end{pmatrix} \tag{1.2}$$

In this book, we follow the standard convention for all matrices, that the elements $a_{i1}, a_{i2}, \ldots, a_{in}$ are the elements of the ith row, and the elements $a_{1j}, a_{2j}, \ldots, a_{mj}$ are the elements of the jth column. That is, the first subscript for an element denotes the column and the second subscript gives the row. Equation 1.2 transforms the components of a vector referred to one basis to those referred to the other basis as:

$$\begin{aligned} a_1 &= R_{11}b_1 + R_{21}b_2 + R_{31}b_3 \\ a_2 &= R_{12}b_1 + R_{22}b_2 + R_{32}b_3 \\ a_3 &= R_{13}b_1 + R_{23}b_2 + R_{33}b_3 \end{aligned} \tag{1.3}$$

In Eq. 1.3, R_{23}, for example, is the second element in the third row (or, equivalently, the third element of the second column) of Eq. 1.2. For $r_1 = r_2 = r_3 = 0.5773$ and $\theta = 60^\circ$, Eq. 1.2 gives:

$$\mathbf{R} = \begin{pmatrix} 0.6667 & 0.6667 & 0.3333 \\ -0.3333 & 0.6667 & 0.6667 \\ 0.6667 & 0.3333 & 0.6667 \end{pmatrix} \tag{1.4}$$

In order to obtain the equivalent axis-angle pairs, $\mathbf{R}$ must be multiplied by the matrices representing the 24 rotation operations of the cubic lattice. The rotational degeneracy of all crystal lattices can be obtained from the character tables for their respective point groups: cubic, O_h (24), hexagonal, D_{6h} (12), hexagonal close packed, D_{3d} (6), tetragonal, D_{4h} (8), trigonal, D_{3d} (6), orthorhombic, D_{2h} (4), monoclinic, C_{2h} (2), and triclinic, C_i (1).

Continuing with the present example, we can operate on Eq. 1.4 with the (3×3) square matrix representing, say, a 90° right-hand rotation about [100], which is obtained from Eq. 1.2 with $r_1 = 1$, $r_2 = r_3 = 0$ and $\theta = 90^\circ$. The result is a product matrix, which we call $\mathbf{J}$:

$$\begin{aligned} \mathbf{J} &= \begin{pmatrix} 1 & 0 & 0 \\ 0 & 0 & 1 \\ 0 & -1 & 0 \end{pmatrix} \begin{pmatrix} 0.6667 & 0.6667 & -0.3333 \\ -0.3333 & 0.6667 & 0.6667 \\ 0.6667 & -0.3333 & 0.6667 \end{pmatrix} \\ &= \begin{pmatrix} 0.6667 & 0.6667 & -0.3333 \\ 0.6667 & -0.3333 & 0.6667 \\ 0.3333 & -0.6667 & -0.6667 \end{pmatrix} \end{aligned} \tag{1.5}$$

Note that **J** is *not* the product of two symmetry operations, because the first rotation took crystal *A* into crystal *B*, rather than back into itself. The *A* and *B* orientations are distinguishable. We can now use **J** to extract an equivalent axis-angle pair. The new rotation angle, θ, is given by

$$j_{11} + j_{22} + j_{33} = 1 + 2\cos\theta \tag{1.6}$$

where the terms on the left-hand side are the diagonal elements of **J**. The equivalent rotation axis for $\theta \neq \pi$ or, for nonsymmetric matrices (when ${}^t\mathbf{J} \neq \mathbf{J}$), is obtained from the relations:

$$r_1 = [j_{23} - j_{32}]/2\sin\theta, \qquad r_2 = [j_{31} - j_{13}]/2\sin\theta, \qquad r_3 = [j_{12} - j_{21}]/2\sin\theta \tag{1.7}$$

where $r_1^2 + r_2^2 + r_3^2 = 1$. When the product matrix is symmetric (${}^t\mathbf{J} = \mathbf{J}$), for example, if $\theta = 180°$, Eq. 1.6 does not apply. In this case, the following equation is needed to determine the rotation matrix:

$$\begin{array}{lll} j_{11} = 1 - 2(r_2^2 + r_3^2) & j_{12} = 2r_1r_2 & j_{13} = 2r_1r_3 \\ j_{21} = 2r_1r_2 & j_{22} = 1 - 2(r_1^2 + r_3^2) & j_{23} = 2r_2r_3 \\ j_{31} = 2r_1r_3 & j_{32} = 2r_2r_3 & j_{33} = 1 - 2(r_1^2 + r_2^2) \end{array} \tag{1.8}$$

where $r_1^2 + r_2^2 + r_3^2 = 1$. When using Eq. 1.8, the idea is to extract the maximum component from the diagonal elements of the matrix. If j_{11} is of maximum magnitude, compute:

$$r_1 = [j_{11} - j_{22} - j_{33} + 1]^{1/2}/2 \qquad r_2 = j_{13}/2r_1 \qquad r_3 = j_{13}/2r_1$$

If j_{22} is the maximum, compute:

$$r_2 = [j_{22} - j_{11} - j_{33} + 1]^{1/2}/2 \qquad r_1 = j_{12}/2u_2 \qquad r_3 = j_{23}/2r_2$$

If j_{33} is the maximum, compute:

$$r_3 = [j_{33} - j_{11} - j_{22} + 1]^{1/2}/2 \qquad r_1 = j_{13}/2r_3 \qquad r_2 = j_{23}/2r_3$$

Example 1.1 Calculate the axis-angle pair from the product matrix in Eq. 1.5 that is equivalent to a 60° rotation about $[111]_A$.

Solution The rotation angle, using Eq. 1.6, is

$$\cos^{-1}([0.6667 - 0.3333 - 0.6667 - 1]/2) = \theta = 2.300\,\text{rad}$$
$$2.3000 \times 180/\pi = 131.8°$$

TABLE 1.2 Axis-Angle Pairs Equivalent to a 60° Rotation about $\langle 111 \rangle_A$ in a Cubic Bicrystal

Axis	Angle
$\langle 111 \rangle_A$	180°
$\langle 012 \rangle_A$	131.8°
$\langle 112 \rangle_A$	180°
$\langle 113 \rangle_A$	146.4°
$\langle 11\bar{3} \rangle_A$	146.4°
$\langle 011 \rangle_A$	70.5°
$\langle 011 \rangle_A$	109.5°

We see by inspection that $\mathbf{J}$ is a nonsymmetric matrix ($j_{ij} \neq j_{ji}$). Therefore, we can use Eq. 1.7 to compute the components of the rotation axis:

$$r_1 = [0.6667 - (-0.6667)]/2 \sin(131.8) = 0.8943$$
$$r_2 = [0.3333 - (-0.3333)]/2 \sin(131.8) = 0.4470$$
$$r_3 = [0.6667 - 0.6667]/2 \sin(131.8) = 0$$

From vector algebra, we know that any ordered set of three numbers that can be obtained from $[r_1\ r_2\ r_3]$ by multiplying all of them by the same positive constant k is also a set of direction numbers for the vector $\boldsymbol{r}$, in that they define the direction of the vector. Hence choosing k to be (1/0.4470) gives: [0.8943/0.4470, 0.4470/0.4470, 0] or [210]. Therefore, the equivalent axis-angle pair is rotated by 131.8° about $[210]_A$.

Using the procedure just outlined with other symmetry operations of the cubic lattice, we can calculate other axis-angle pairs that, for the purposes of expressing the orientation relationship in a cubic bicrystal, are equivalent to a 60° rotation about $\langle 111 \rangle_A$. The results are given in Table 1.2

Obviously, a completely unambiguous description of the relative orientation between two identical crystals must contain the axis-angle pair (rather than an angle alone). As we have just seen, however, a rotation matrix can also be used to specify the orientation relation within a bicrystal. We have just gone to great lengths to show how these matrix elements are computed. The advantage of expressing the orientation relationship in this manner will be apparent in Section 1.1.3 where we quantify the "goodness of fit" at the interface between grains.

1.1.2 Grain Boundary Orientations

We have been discussing orientation relationships between pairs of grains. This is *not* the same as the orientation of the grain boundary. For example, Figure 1.1 shows a twinned bicrystal like that discussed earlier. As illustrated in the figure, the grain boundary plane between two crystals with this orientation relationship need not coincide with the twin plane. The orientation relationship between the grains

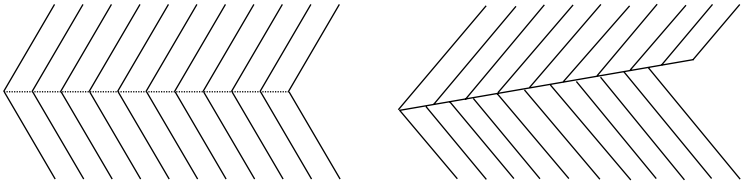

(*a*) (*b*)

Figure 1.1 (a) The twin plane coincides with the boundary plane. (b) The twin plane and boundary plane do not coincide.

does provide us with three of the five degrees of freedom needed to specify the grain boundary orientation, however. One of these degrees of freedom, we have seen, is a rotation angle. The rotation is carried out about a rotation axis, which we have been denoting by three indices of direction, [*uvw*]. Because an axis is a polar vector in spherical coordinates, it can also be specified by a polar angle and an azimuthal angle relative to the grain boundary plane. Thus, three of our five degrees of freedom are Euler angles that, taken together, describe the orientation relationship between the grains: $0 \leq \phi_E \leq 2\pi$; $0 \leq \theta_E \leq \pi$; and $0 \leq \psi_E \leq 2\pi$ (the subscript E simply denotes that these are Euler angles). The remaining two degrees of freedom define the boundary plane in the coordinate system of the reference grain. They are spherical angles that specify the boundary plane inclination: $0 \leq \theta_S \leq 2\pi$; $0 \leq \phi_S \leq \pi$, where the subscript S denotes spherical angles.

One might naturally ask: How many different grain boundary orientations are observable? The number of distinguishable orientations, N, depends on the precision with which the various angular measurements are made, and the number of symmetry operators for the crystal class. For example, for a cubic bicrystal the boundary normal can be selected in two directions, the crystals can be exchanged, and one can apply 24 rotation operations to either crystal. There are thus $2 \cdot 2 \cdot 24^2$ combinations of the five angular parameters that lead to identical bicrystals. To generalize, if we represent the number of symmetry operations for the crystal class by η, the precision of the angular measurements by Δ, and the number of degrees of freedom by n, we have the following formula for the number of distinguishable orientations (Saylor et al., 2000).

$$\begin{aligned} N &= 1/(4\eta^2)\prod_{n,\Delta}(n/\Delta) \\ &= [(2\pi)(\pi)(2\pi)(2\pi)(\pi)]/(4\eta^2\Delta^5) \\ &= 8\pi^5/(4\eta^2\Delta^5) \end{aligned} \tag{1.9}$$

where Δ is in radians. The $8\pi^5$ factor is the product of the full ranges for each angular parameter. For a cubic system, if $\Delta = 0.087$ (5°), Eq. 1.9 predicts 2.1×10^5 distinct boundaries. The number of distinguishable boundaries obviously increases with increases in the angular precision.

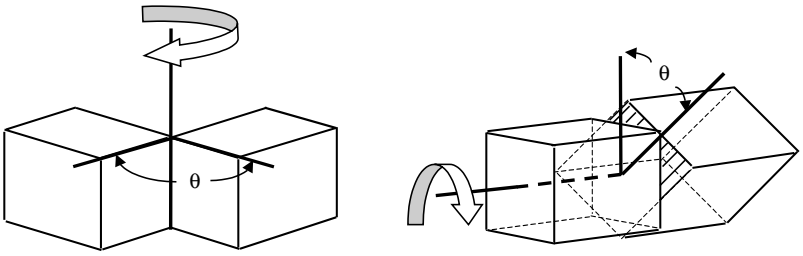

Figure 1.2 (a) A tilt boundary. (b) A twist boundary.

Despite such a large number of possible orientations, it has been observed experimentally that grain orientation relationships do not occur in a random manner. For example, low-energy grain boundaries like the twin boundary are very commonly observed in cubic systems. It is hard to say whether this is a result of thermodynamic or kinetic control. Interfacial energy minimization could be responsible, or the activation energies for nucleation and grain growth in certain orientations could be lower, or possibly both factors could be at work.

The Dislocation Model of Low Angle Grain Boundaries A general grain boundary has a mixture of *tilt* and *twist* character. We can think of a pure tilt boundary as consisting of an axis of rotation that is in the grain boundary plane (Figure 1.2a). In contrast, twist boundaries contain an axis of rotation that is perpendicular to the grain boundary plane (Figure 1.2b). A useful way to picture the symmetrical tilt boundary (a boundary in which the boundary plane contains the rotation axis and bisects the rotation angle) is to consider it as a straight array of *edge dislocations*, as in Figure 1.3. In a single-crystal metal, edge dislocations consist of extra half-planes of atoms. In ionic or covalent crystals, edge dislocations involve extra half planes of unit cells. As long as the misorientation angle is low (i.e., small-angle grain boundaries), tilt boundaries may be regarded as the coalescence of these line defects into a dislocation network. The spacing between the dislocations, D, is

$$D = \boldsymbol{b} / \sin \theta \tag{1.10}$$

where $\boldsymbol{b}$ is the *Burgers vector*, perpendicular to the line of the dislocation, and θ is the misorientation angle.

If the dislocation density is low (the value of D is large), a semicoherent interface results, in which regions of good fit are separated by the individually recognizable interface dislocations. Note how the extra half-planes in Figure 1.3 all have a single Burgers vector. In an unsymmetrical low-angle tilt boundary, different Burgers vectors are required to accommodate the mismatch. The dislocation model is really only valid for low-angle grain boundaries. In the cubic crystal class, for

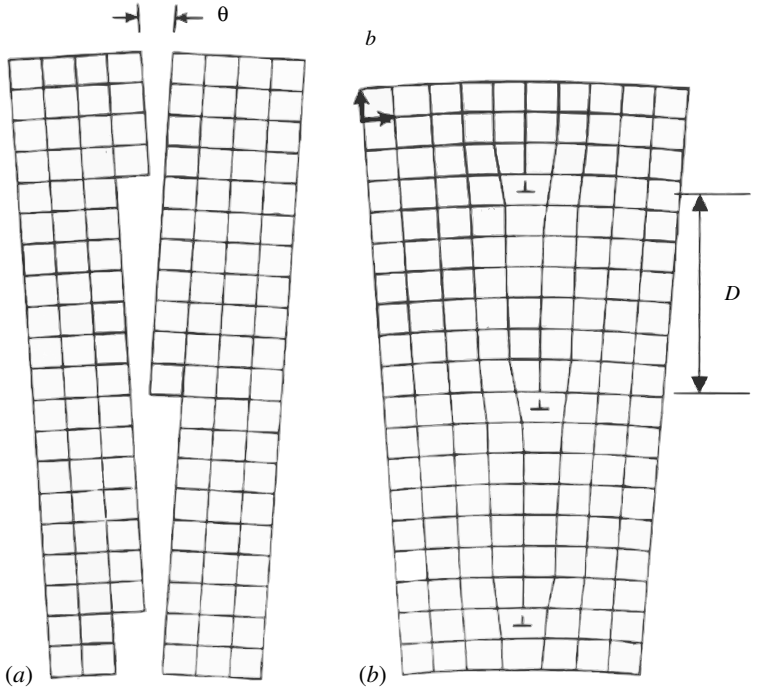

Figure 1.3 (a) A low-angle tilt boundary. (b) Representation as an array of parallel edge dislocations.

values $\theta > \sim 15^\circ$, D can get so small, corresponding to a high dislocation density, that dislocations become indistinguishable (Read and Shockley, 1950). The symmetrical low-angle twist boundary can similarly be represented by a screw dislocation (Figure 1.4). Screw dislocations have been likened to multistoried parking garages, the atomic planes spiraling around the dislocation line in the same

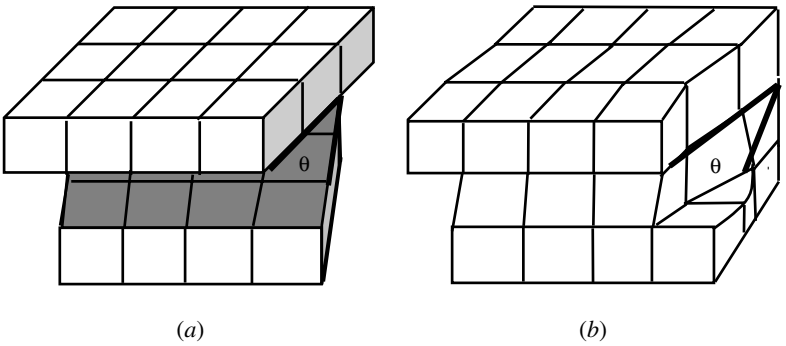

Figure 1.4 (a) A low-angle twist boundary. (b) Representation as a screw dislocation.

manner as a parking garage floor spirals around a central pole of the garage (Weertman and Weertman, 1992).

1.1.3 Grain Boundary Geometry: The Coincidence Site Lattice

The evolution of our modern picture of crystalline interfaces can be summarized as follows. The earliest geometric models of crystalline interfaces were the ''amorphous'' high-angle grain boundary by Hargreaves and Hill (Hargreaves and Hill, 1929), and the twin interface by the French mining engineer and crystallographer Georges Friedel (1865–1933) (Friedel, 1926), son of organic chemist Charles Friedel. (1832–1899). N. F. Mott first suggested that grain boundaries should contain regions of fit and misfit (Mott, 1948). Kronberg and Wilson then pointed out the importance of the coincidence of atom positions across grain boundaries in influencing metal properties such as diffusion coefficients and mobilities (Kronberg and Wilson, 1949). Ranganthan presented a general procedure for obtaining coincidence relationships between lattices about rotation axes (Ranganathan, 1966).

The modern method for quantifying the goodness of fit between two adjacent grains examines the number of lattice points (*not* atomic positions) from each grain that coincide. In special cases, for example when the grain boundary plane is a twin plane, the lattice sites for each of the adjacent crystals coincide *in* the boundary. These are called *coherent* boundaries. It has long since been experimentally verified that coherent grain boundaries possess special properties. For example, coherent boundaries migrate faster than random boundaries during recrystallization (Aust and Rutter, 1959).

Consider a pair of adjacent crystals. We mentally expand the two neighboring crystal lattices until they interpenetrate and fill all space. Without loss of generality, it is assumed that the two lattices possess a common origin. If we now hold one crystal fixed and rotate the other, it is found that a number of lattice sites for each crystal, in addition to the origin, coincide with certain relative orientations. The set of coinciding points form a *coincidence site lattice*, or CSL, which is a sublattice for both the individual crystals.

In order to quantify the lattice coincidence between the two grains, A and B, the symbol Σ customarily designates the reciprocal of the fraction of A (or B) lattice sites that are common to both A and B.

$$\Sigma = \text{Number of crystal lattice sites}/\text{Number of coincidence lattice sites} \quad (1.11)$$

For example, if one-third of the A (or B) crystal lattice sites are coincidence points belonging to both the A and B lattices, then, $\Sigma = 1/(1/3) = 3$. The value of Σ also gives the ratio between the areas enclosed by the CSL unit cell and crystal unit cell. The value of Σ is a function of the lattice types and grain misorientation. The two grains need not have the same crystal structure or unit cell parameters. Hence, they need not be related by a rigid-body rotation. The boundary plane intersects the CSL and will have the same periodicity as that portion of the CSL along which the intersection occurs.

The simple CSL model is directly applicable to the cubic crystal class. The lower symmetry of the other crystal classes necessitates the more sophisticated formalism known as the *constrained coincidence site lattice*, or CCSL (Chen and King, 1988). In this book, we only treat cubic systems. Interestingly, whenever an *even* value is obtained for Σ in a cubic system, it will always be found that an additional lattice point lies in the center of the CSL unit cell. The true area ratio is then half the apparent value. This operation can always be applied in succession, until an odd value is obtained—thus Σ is always *odd* in the cubic system. A rigorous mathematical proof of this would require that we invoke what is known as O-lattice theory (Bollman, 1967) The O-lattice takes into account all equivalence points between two neighboring crystal lattices. It includes as a subset not only coinciding lattice points (the CSL) but also all nonlattice sites of identical internal coordinates. However, to expand on that topic would be well beyond the scope of this textbook. The interested reader is referred to Bhadeshia (1987) or Bollman (1970).

Single crystals and bicrystals with no misorientation (i.e., $\theta = 0$), by convention, are denoted $\Sigma 1$. In practice, small- or low-angle grain boundaries with a misorientation angle less than 10°–15° are also included under the $\Sigma 1$ term. Since Σ is always odd, the coincidence orientation for high-angle boundaries with the largest fraction of coinciding lattice points is $\Sigma 3$ (signifying that 1/3 of the lattice sites coincide). Next in line would be $\Sigma 5$, then $\Sigma 7$, and so on.

Figure 1.5 shows a tilt boundary between two cubic crystals. The grain boundary plane is perpendicular to the plane of the page. In the figure, we are looking down one of the $\langle 100 \rangle$ directions, and the [100] axis about which grain *B* is rotated is also perpendicular to the page and passes through the origin. At the precise misorientation angle of 36.9°, one-fifth of the *B* crystal lattice sites are coincidence points, which also belong to the expanded lattice of crystal *A*; this is a $\Sigma 5$ CSL misorientation. The set of coincidence points forms the CSL, the unit cell of which is outlined. Note that the area enclosed by the CSL unit cell is five times that enclosed by the crystal unit cell.

Fortunately, there is an easy, although tedious, way to determine the true value for Σ. If an integer, *N*, can be found such that all the elements of the rotation matrix become integers when multiplied by *N*, then that integer will be the Σ value. The value of *N* is found simply by multiplying all the matrix elements by integers, in increments of one beginning with the number 1, until the matrix elements are all integers. If the value of Σ turns out to be even using this procedure, then the true value is obtained by successively dividing *N* by two until the result is an odd integer. This method can be used to compute the value of Σ for any general rotation matrix. For example, factoring out 1/3 from $\mathbf{R}$ in Eq. 1.4 gives a matrix with integral elements, in which Σ is equal to three:

$$\mathbf{R} = 1/3 \begin{pmatrix} 2 & 2 & -1 \\ -1 & 2 & 2 \\ 2 & -1 & 2 \end{pmatrix}$$

Hence, the 60° $\langle 111 \rangle$ twin boundary has a $\Sigma 3$ CSL misorientation. It is also a coherent boundary because of the large number of coincidence points along the

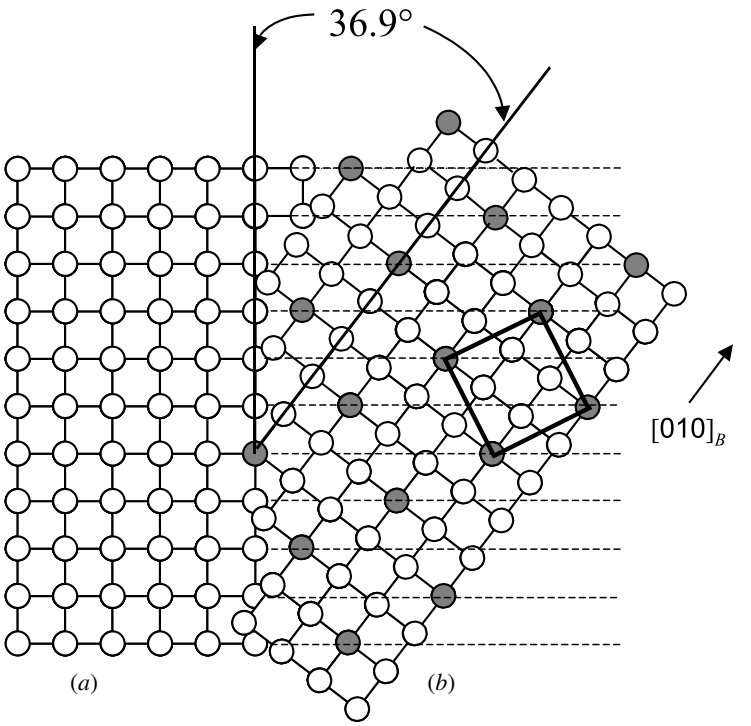

Figure 1.5 A view down the [001] direction of a tilt boundary between two crystals (A, B) with a misorientation angle of 36.9° about [001]. The grain boundary is perpendicular to the plane of the page. Every fifth atom in the [010] direction in B is a coincidence point (shaded). The area enclosed by the CSL unit cell (bold lines) is five times that of the crystal unit cell, so $\Sigma = 5$.

twin plane itself, as shown in Figure 1.6. In this figure, we are looking down *on* the $\langle 111 \rangle$ rotation axis. The lattice sites shown are in rows off the $\langle 111 \rangle$ axis, along the set of (111) planes, as illustrated in the bottom left corner. It will be recalled that the boundary plane intersects the CSL and will have the same periodicity as that portion of the CSL along which the intersection occurs. Thus, not all $\Sigma 3$ boundaries will be coherent. For example, although rotations of 70.5° and 109.5° about $\langle 011 \rangle_A$ are also equivalent $\Sigma 3$ misorientations, only the 70.5° rotation will result in a high degree of coincidence along the $\langle 011 \rangle$.

Example 1.2 The matrix corresponding to a rotation of 50.5° about [110] is given in Bhadeshia's monograph *Worked Examples in the Geometry of Crystals* as:

$$\mathbf{R} = \begin{pmatrix} 0.545621 & -0.545621 & 0.636079 \\ 0.181961 & 0.818039 & 0.545621 \\ 0.818039 & 0.181961 & -0.545621 \end{pmatrix}$$

Calculate the value of Σ.